

Article

Nb-Modified Ce/Ti Oxide Catalyst for the Selective Catalytic Reduction of NO with NH₃ at Low Temperature

Jawaher Mosrati ¹, Hanan Atia ², Reinhard Eckelt ², Henrik Lund ² , Giovanni Agostini ², Ursula Bentrup ², Nils Rockstroh ² , Sonja Keller ², Udo Armbruster ^{2,*} and Mourad Mhamdi ^{1,3}

¹ Laboratoire de Chimie des Matériaux et Catalyse, Departement de Chimie, Faculté des Sciences de Tunis, Campus Universitaire El Manar, 2092 El Manar Tunis, Tunisia; Jawahermosrati98@gmail.com (J.M.); mourad.mhamdi@gmail.com (M.M.)

² Leibniz-Institut für Katalyse e.V., Albert-Einstein-Strasse 29a, 18059 Rostock, Germany; hanan.atia@catalysis.de (H.A.); reinhard.eckelt@catalysis.de (R.E.); henrik.lund@catalysis.de (H.L.); giovanni.agostini@catalysis.de (G.A.); ursula.bentrup@catalysis.de (U.B.); nils.rockstroh@catalysis.de (N.R.); sonja.keller@catalysis.de (S.K.)

³ Institut Supérieur des Technologies Médicales de Tunis, Université de Tunis El Manar, 9 Rue Zouhaier Essafi 1006 Tunis, Tunisia

* Correspondence: udo.armbruster@catalysis.de; Tel.: +49-381-1281-257

Received: 9 March 2018; Accepted: 23 April 2018; Published: 26 April 2018



Abstract: Recently, great attention has been paid to Ceria-based materials for selective catalytic reduction (SCR) with NH₃ owing to their unique redox, oxygen storage, and acid-base properties. Two series of bimetallic catalysts issued from Titania modified by Ce and Nb were prepared by the one-step sol-gel method (SG) and by the sol-gel route followed by impregnation (WI). The resulting core-shell and bulk catalysts were tested in NH₃-SCR of NO_x. The impregnated Nb5/Ce40/Ti100 (WI) catalyst displayed 95% NO_x conversion at 200 °C (GHSV = 60,000 mL·g⁻¹·h⁻¹, 1000 ppm NO_x, 1000 ppm NH₃, 5% O₂/He) without forming N₂O. The catalysts were characterized by various methods including ICP-OES, N₂-physisorption, XRD, Raman, NH₃-TPD, DRIFTS, XPS, and H₂-TPR. The results showed that the introduction of Nb decreases the surface area and strengthens the surface acidity. This behavior can be explained by the strong interaction between Ceria and Titania which generates Ce-O-Ti units, as well as a high concentration of amorphous or highly dispersed Niobia. This should be the reason for the excellent performance of the catalyst prepared by the sol-gel method followed by impregnation. Furthermore, Nb5/Ce40/Ti100 (WI) has the largest NH₃ adsorption capacity, which is helpful to promote the NH₃-SCR reaction. The long-term stability and the effect of H₂O on the catalysts were also evaluated.

Keywords: low-temperature SCR; Ceria-based catalysts; Niobia; sol-gel method

1. Introduction

Nitrogen oxides (NO_x), emitted from the industrial combustion of fossil fuels and automobile exhaust gas, are major air pollutants leading to various environmental problems: acid rain, photochemical smog, ozone depletion, and the greenhouse effect [1–3]. The steady increase of NO_x emissions necessitates the improvement of abatement technologies. The selective catalytic reduction (SCR) is the most promising way to remove NO_x from stationary sources and vehicles exhaust gas [4–6]. A reducing agent is needed to convert NO_x into inert components like water and nitrogen. For this purpose, mostly urea is used for fixed stations (nitric acid plants); however, it is also used in catalytic reactors fitted to diesel engines and some vessels because of the high NO_x conversions that can be

achieved at a high space velocity [4]. Nowadays, TiO₂ (anatase) supported V₂O₅-WO₃ or V₂O₅-MoO₃ oxides have been commercialized for stationary applications [2,7]. V₂O₅ is the main redox active site, whereas WO₃ (or MoO₃) promotes the surface acidity [2,8]. However, some drawbacks of vanadium-based catalysts were observed during industrial application, such as the biological toxicity and volatility of V₂O₅, the narrow operating temperature window (300–400 °C), and high activity for the oxidation of SO₂ to SO₃ [9–11]. As an alternative, low-temperature catalysts—if available—could be placed downstream of electrostatic precipitator and desulfurization units. Therefore, it is crucial to develop novel, environment-friendly, and non-vanadium-based catalysts with high NO_x conversion, high N₂ selectivity, nontoxic species, and high resistance to H₂O for NH₃-SCR.

Ceria-based materials are of particular interest for NH₃-SCR owing to their redox cycle between Ce³⁺ and Ce⁴⁺, ability for oxygen storage, and acid-base properties [12,13]. Ceria is not very toxic and comparatively cheap. Therefore, Ceria has already been widely used as an indispensable component in automotive three-way catalysts. Recently, many researchers studied the effect of introducing solid acid components on NH₃-SCR catalysts such as CeO₂-TiO₂ [14,15], CeO₂-WO₃ [16–22], CeO₂-SO₄²⁻ [23–25], CeO₂-Nb₂O₅ [26–30], CeO₂-PO₄³⁻ [31,32], and CeO₂-MoO₃ [33]. Additionally, CeO₂ was reported to have the ability to resist SO₂ and alkali poisoning [34].

Among them, CeO₂-Nb₂O₅-based catalysts offer high potential for diesel exhaust gas treatment due to their multi-functionality, such as the hydrolysis of urea to NH₃, the SCR of NO_x with NH₃, and the oxidation of soot [28–30]. Binary oxides of Cerium and Niobium were reported to improve the acidity of catalysts, which was suggested to be an important feature in the NH₃-SCR reaction [29]. Niobium modification in general appears to be an effective strategy in selective catalytic reduction of NO_x with ammonia or hydrocarbons [29,30]. The Nb–OH bond is the source for Brønsted acid sites and the Nb=O bond for Lewis acid sites, both of which are essential in the NH₃-SCR reaction [29]. The positive effect of modifying the acidic properties with NbO_x and the generation of structural defects in Ce-Nb (oxygen vacancies) increase the electron conductivity [29,30,35,36]. So, the combination of the Nb₂O₅ acid properties and the redox behavior of CeO₂ may lead to a good SCR performance. Despite the availability of some data from these studies on SCR performance in different reaction conditions, an understanding of the structure-activity relationship of CeO₂-Nb₂O₅-TiO₂ catalysts is still missing, e.g., the correlation of De-NO_x activity to surface acidity and redox ability.

Regarding the successful application of TiO₂ as a support in V₂O₅-WO₃/TiO₂ and V₂O₅-MoO₃/TiO₂ catalysts for NH₃-SCR and the potential of the CeO₂-Nb₂O₅ catalyst for the SCR of NO_x, it is of great interest to study a combination of them. The NH₃-SCR performance of NO_x on this type of supported metal oxide has not yet been studied.

In the present study, we synthesized Ce₄₀/Ti₁₀₀ (numbers indicate elemental ratios) and Nb₅/Ce₄₀/Ti₁₀₀ catalysts (Nb given in weight percent) by the one-step sol-gel method or by the impregnation of support Ce₄₀/Ti₁₀₀ with Niobia and their efficiency in the low-temperature NH₃-SCR was elucidated. The beneficial effect of Nb and Ce on NO conversion and N₂ selectivity will be demonstrated and explained.

2. Results

2.1. NH₃-SCR Performance

The results from NH₃-SCR runs with different catalysts are given in Figure 1a,b, including some blank tests. The reference materials TiO₂ (support) and Nb₅/Ti₁₀₀ (Ceria-free catalyst, 5 wt % Nb) were inactive below 300 °C; first upon raising the temperature to 400 °C, the conversion increased to 15 and 30%, respectively. On the other hand, the NO_x conversion with the Nb-free Ce₄₀/Ti₁₀₀ (SG) catalyst showed a remarkable increase with temperature, reaching 78% at 200 °C and 99% at 300 °C. Presence of Ceria is essential for high SCR activity.

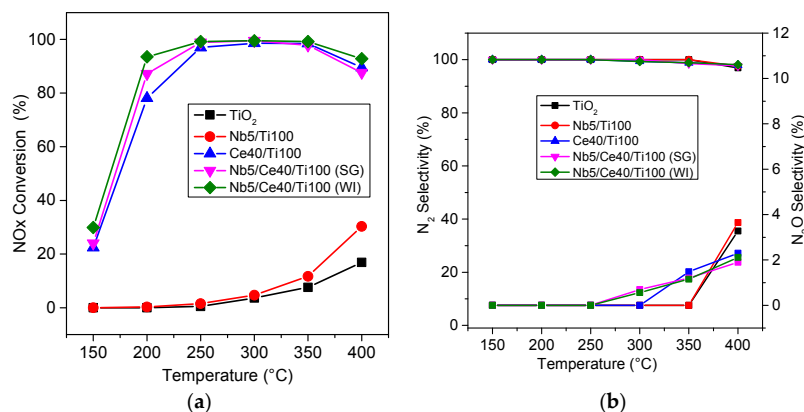


Figure 1. (a) NO_x conversion and (b) N₂-N₂O selectivity for different catalysts (1000 ppm NO_x, 1000 ppm NH₃, 5% O₂/He, GHSV = 60,000 mL·g⁻¹·h⁻¹).

Both catalysts Nb5/Ce40/Ti100 (SG) and Nb5/Ce40/Ti100 (WI) outnumbered all these reference materials and showed almost complete conversion of NO_x at 250 °C. At 200 °C, the Nb5/Ce40/Ti100 (WI) catalyst was more active and exhibited 95% NO_x conversion, while Nb5/Ce40/Ti100 (SG) showed 87%. Even at 150 °C, the Nb5/Ce40/Ti100 (WI) showed higher conversion (30%) than Nb5/Ce40/Ti100 (SG) (24%) and Ce40/Ti100 (22%). A similar system with 20% CeO₂/TiO₂ prepared by an impregnation method was reported elsewhere, which affords 95% conversion in the range of 250–375 °C at a GHSV of 25,000 h⁻¹ [15]. However, on setting the GHSV to 50,000 h⁻¹, still being lower than the value applied in the present paper (60,000 mL·g⁻¹·h⁻¹), a much higher temperature of 350 °C was needed to reach 97% conversion. A comparison of three preparation methods for CeO₂/TiO₂ catalysts revealed that only the catalyst prepared by a single step sol-gel method showed complete conversion at 225 °C and GHSV = 50,000 h⁻¹ [34]. In addition, the Ce-Nb system with a ratio of 1:1 prepared with the co-precipitation method presented 80% NO conversion in a temperature range of 200–450 °C with a GHSV = 120,000 mL·g⁻¹·h⁻¹ [29]. A ternary oxide system Mn/Ce/Nb/Ti exhibited complete NO_x conversion at 150 °C at a high GHSV of 180,000 h⁻¹ [37]. Mn-Ce oxide catalysts were found to allow complete conversions at 100–150 °C at a space velocity of 42,000 h⁻¹ but showed considerable deactivation in the presence of 19% H₂O [38]. The present catalyst does not reach such high values at these temperatures. However, Mn-based catalysts, due to their oxidative power, promoted the formation of undesired products N₂O and NO₂ [37]. It can be first pointed out that the addition of Nb to Ce-TiO₂ improves the NO_x conversion particularly at temperatures below 250 °C and in the absence of H₂O, and a clear synergistic effect exists between Nb, Ce, and Ti species. Regarding these data, the presented catalyst Nb5/Ce40/Ti100 (WI) appears to be an attractive intermediate temperature catalyst as it avoids the over-oxidation as known from Mn catalysts. Furthermore, it shows higher activity than conventional V₂O₅/TiO₂. In conclusion, Nb5/Ce40/Ti100 (WI) showed highly competitive results comparable to the state-of-art. Second, the applied preparation methods seem to have a significant effect on the catalyst efficiencies.

The N₂ selectivity with Nb5/Ce40/Ti100 (WI) reaches 100% below 250 °C and exceeds 99% within the whole temperature range, as shown in Figure 1b; this indicates that the interaction of Nb species with Ce40/Ti100 (SG) suppresses the unselective catalytic oxidation of NH₃ by O₂ towards N₂O and NO₂ at high temperature, as it was observed elsewhere [29,37]. The N₂O concentration recorded with these catalysts is especially low (<2.5%) at 300–400 °C.

Water vapor is an inevitable compound in automotive exhaust gases and always significantly influences the catalytic activity. To investigate the long-term stability and the effect of water (8 vol %) on the performance of the catalysts, runs were made at 200 °C to apply technically relevant conditions for low-temperature SCR.

When adding 8 vol % of water to the gas flow during catalyst testing, the conversion drops by 22% for Nb5/Ce40/Ti100 (WI) and by 27% for both Ce40/Ti100 and Nb5/Ce40/Ti100 (SG). Within the first 4 h on stream Nb5/Ce40/Ti100 (WI) showed a slight decrease in conversion from 65 to 62% (Figure 2). Upon switching off the water dosage, the NO_x conversion rapidly recovered to 85%, indicating that the inhibition effect of water is largely reversible. However, the initial conversion of 95% (Figure 1a) was not recovered probably due to some minor structural changes which could occur in the presence of water, causing a deactivation of the catalyst. Nevertheless, on switching on H₂O again, the conversion recovered, reached its initial value of 62%, and then decreased slowly to 60% over 12 h. Surprisingly, Ce40/Ti100 displayed during the first 4 h on stream comparable activity as Nb5/Ce40/Ti100 (SG) and even appeared more stable over 12 h. In general, the catalysts deactivate in the presence of H₂O, but Nb5Ce40Ti100 (WI) is less pronounced deactivated compared to the others. This can be explained by the competitive adsorption between NH₃/NO_x and H₂O on the active sites, leading to an inhibiting effect of H₂O on the low-temperature SCR reaction [39,40].

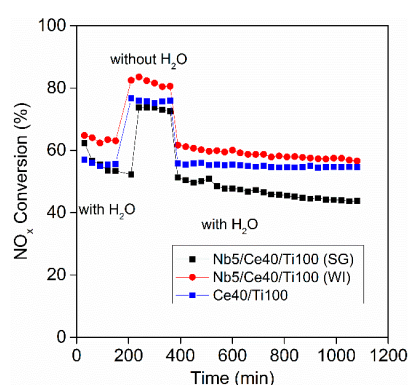


Figure 2. Long-term activity and effect of water on the SCR activity at 200 °C (1000 ppm NO_x, 1000 ppm NH₃, 5 vol % O₂, 8 vol % H₂O, balance He, GHSV = 60,000 mL·g⁻¹·h⁻¹).

2.2. Physicochemical Characterization

2.2.1. Structural and Textural Properties (ICP-OES, BET, XRD, and Raman)

The chemical compositions of the catalysts were analyzed by the ICP-OES technique and the weight percentage of each element is listed in Table 1. The values for Nb are lower than expected for all the catalysts, while for Ce, the content is slightly higher than expected. This can be explained by the method of drying the solvent under supercritical conditions, e.g., by partial leaching of Nb species by this solvent.

The textural properties of the samples were investigated by N₂ adsorption-desorption at 77 K (Table 1). Figure 3a–e show the corresponding N₂ adsorption-desorption isotherms and BJH pore size distributions for the catalysts, respectively. All the catalysts exhibited typical type IV isotherms with an obvious type H3 hysteresis loop as classified by IUPAC, which is always assigned to capillary condensation in mesopores ascribed to the interstices between the particles [41]. The specific BET surface area of the chosen TiO₂ support was 141 m²·g⁻¹ and a loss of 15% was observed upon impregnating with NbCl₅ (WI). After sol-gel preparation with CeO₂, the TiO₂ supported sample lost 36% of its surface. Addition of Nb during the sol-gel (SG) technique did not cause any decrease in surface area, while by impregnation, the surface area decreased to 56 m²·g⁻¹ as expected due to the blocking of pores. While the addition of Ce to Ti in the sol-gel formation of the support leads to a loss in BET surface area, the modification of the preparation method by adding Nb as a third component seems to enlarge the BET surface area, as well as the pore volumes and diameters. This might be explained by the incorporation of Nb in the framework formed by Ce and Ti species. In contrast, after impregnation of the sol-gel-based Ce40/Ti100 with Nb, parts of the pores are blocked. The average pore diameters

of all samples are between 5 and 10 nm (Figure 3b), which confirms that mesopores account for the dominant role in the catalysts (Table 1).

Table 1. Catalyst composition, specific BET surface area, and pore volume (SG = sol-gel route; WI = wet impregnation).

Catalyst	Element Composition (wt %)			S_{BET} ($m^2 \cdot g^{-1}$)	Pore Volume ($cm^3 \cdot g^{-1}$)	Average Pore Diameter (nm)
	Nb	Ce	Ti			
TiO ₂	-	-	-	141	0.26	5.4
Nb5/Ti100 (WI)	4.3	-	49.1	121	0.26	7.3
Ce40/Ti100 (SG)	-	35.7	28.2	90	0.22	6.9
Nb5/Ce40/Ti100 (SG)	4.1	35.0	26.7	94	0.32	9.8
Nb5/Ce40/Ti100 (WI)	4.6	34.4	26.8	56	0.17	7.1

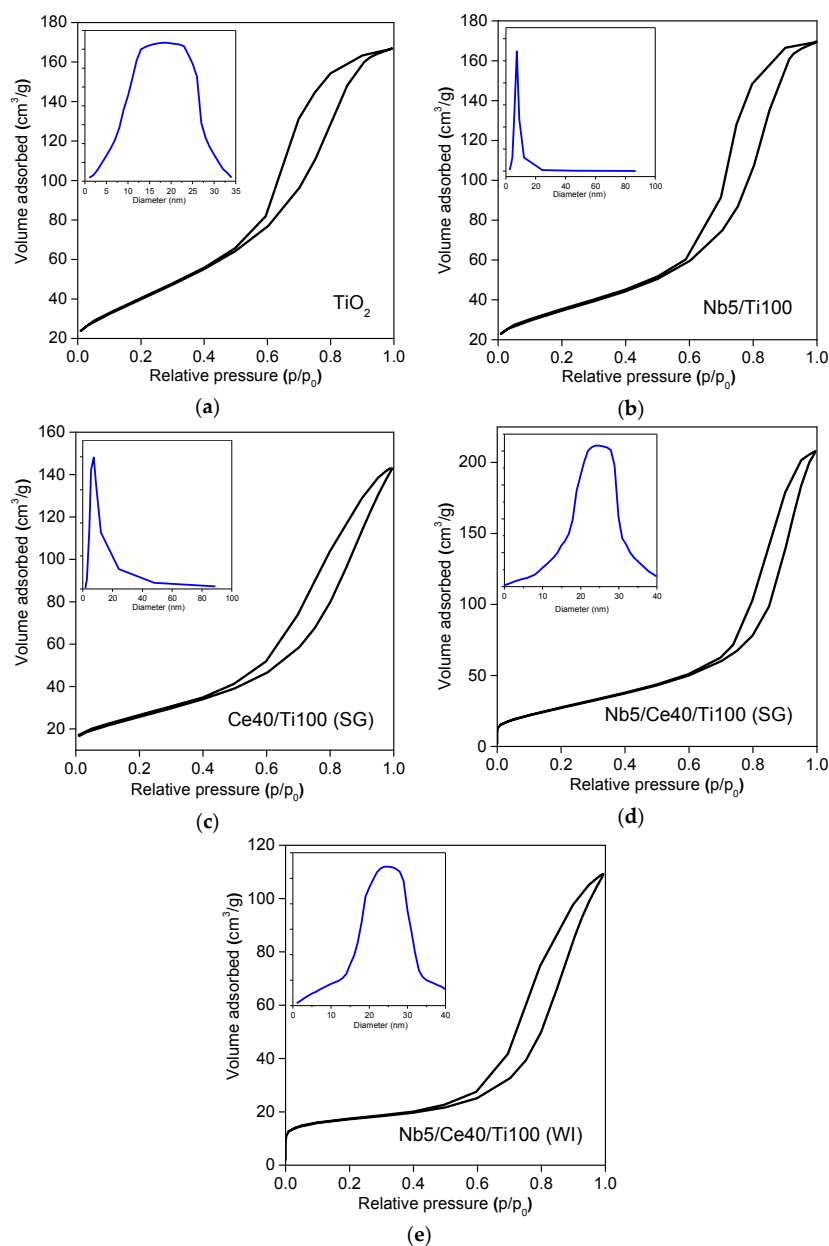


Figure 3. N₂ adsorption-desorption isotherms and BJH pore distributions for all fresh catalysts: (a) TiO₂, (b) Nb5/Ti100, (c) Ce40/Ti100 (SG), (d) Nb5/Ce40/Ti100 (SG), (e) Nb5/Ce40/Ti100 (WI).

The XRD patterns of the catalysts are presented in Figure 4. The powder patterns of the catalysts synthesized from the pure Ti(IV) isopropoxide indicate the presence of anatase modification of Titania (ICDD PDF-2 2017). After the impregnation of TiO₂ with an Nb precursor, no additional reflexes which can be assigned to a Nb-containing phase were observed. Furthermore, no change of the unit cell parameters of anatase was seen. This suggests that the Nb species are highly dispersed on the surface or in an amorphous state. In contrast, the impregnation with Ce precursor leads to the formation of cubic Ceria (Figure 4, triangles) and a non-stoichiometric brannite-like structured Ceria-Titania-oxide (Ce_{0.97}Ti₂O_{5.95}, Figure 4, hereinafter called CeTi₂O₆). Further treatment after impregnation with Niobium species (Nb5/Ce40/Ti100 (SG), Nb5/Ce40/Ti100 (WI)) leads to the loss of crystallinity, as indicated by the additional peak broadening (cf. calculated crystallite sizes, Table 2). In general, the catalyst prepared by the impregnation method was more crystalline than the catalysts obtained via the sol-gel method. As Nb⁵⁺ has a smaller ionic radius (0.064 nm) compared to Ce⁴⁺ (0.087 nm), Nb can diffuse into the lattice of CeO₂ and decrease its crystallinity [42]. This may explain the decrease in Nb5/Ce40/Ti100 (SG) crystallinity compared to the impregnated sample, as due to the homogeneous distribution of the elements it is more likely that Nb interacts with Ce and Ti. This behavior is also proved by the decrease in the crystallite size of CeO₂ and CeTi₂O₆ (Table 2). It is important to note that upon impregnating Ce40/Ti100 with Nb, there was a loss in surface area which enhances the agglomeration and causes an increase in the crystallite size of CeTi₂O₆. These effects were closely related to the catalyst preparation methods. However, the presence of Titania (anatase) can be discussed in all of the three samples which contain Ce as well.

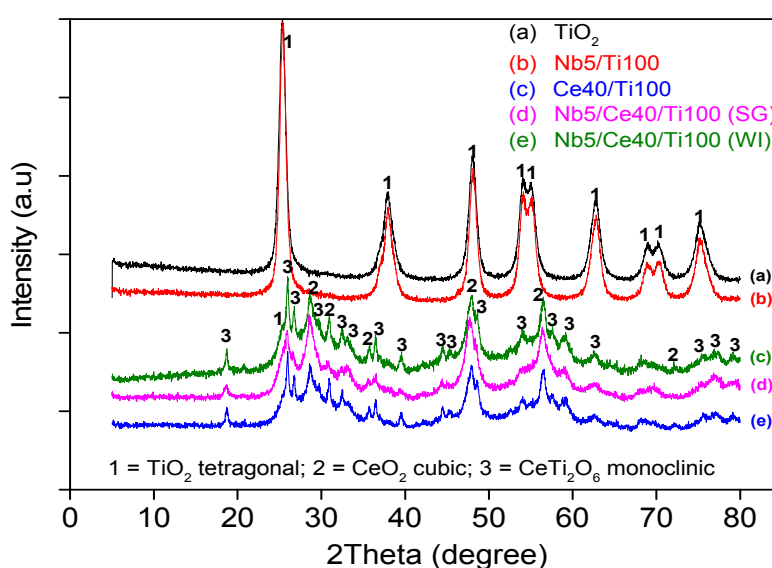


Figure 4. XRD patterns of the fresh catalysts.

Table 2. Crystallite sizes of prepared catalysts calculated with Scherrer's formula [43].

Catalysts	Crystallite Size (nm)		
	CeTi ₂ O ₆	TiO ₂	CeO ₂
Ce40/Ti100	23.5	-	5.6
Nb5/Ce40/Ti100 (SG)	12.6	6.2	4.3
Nb5/Ce40/Ti100 (WI)	18.8	-	7.4

These results are also backed by Raman spectra (Figure 5), wherein all the catalysts show typical bands of TiO₂ (anatase) at 143, 396, 515, and 637 cm⁻¹ [44–46]. These results are in good agreement with XRD data and further confirm that the anatase structure of the TiO₂ support is retained. However,

preparing the mixture of Ce and TiO₂ with the sol-gel technique creates several new bands at 162, 191, 270, 332, 371, 571, and 641 cm⁻¹, which can be assigned to CeTi₂O₆ [47,48]. The formation of such Ce-Ti phases is probably responsible for the improved catalyst performance. The band at 463 cm⁻¹ can be attributed to CeO₂ and/or CeTi₂O₆ phase. No bands for Nb₂O₅ were observed in all of the catalysts, suggesting the high dispersion of Nb species on the surface of Ce40/Ti100. Additionally, it is noticeable for the SG catalyst that the band intensities at 193, 332, 368, 571, and 640 cm⁻¹ are lower compared to the WI sample, which proves that the addition of Niobium decreases crystallinity, thereby confirming the XRD results.

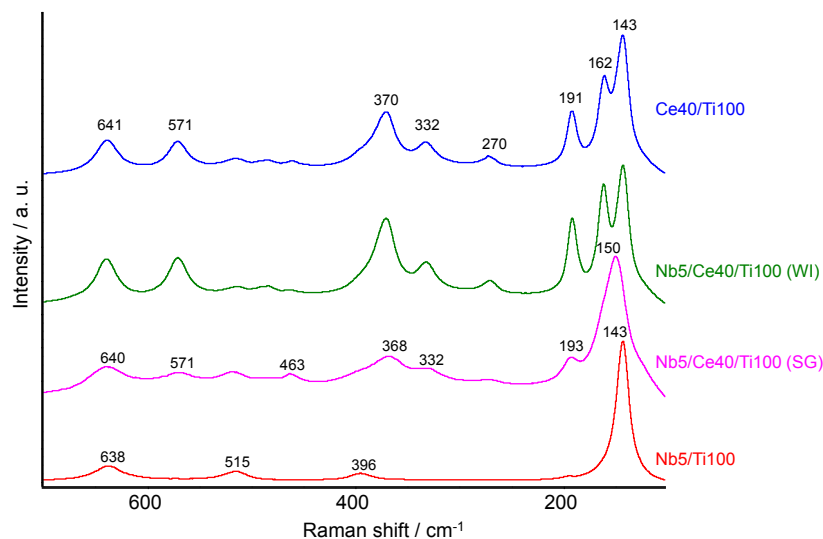


Figure 5. Raman spectra of all fresh samples.

2.2.2. Acid Properties (NH₃-TPD and DRIFTS)

NH₃-TPD runs were carried out to analyse the amount and strength of the acid sites of the materials. These parameters correlate with the position and area of the desorption peak, respectively [49]. As shown in Figure 6, all of the catalysts possess one broad peak ranging from 150 to 500 °C with a maximum around 300 °C. TiO₂ has the highest number of acidic centers (605.7 μmol/g) but they are weak ones (Table 3). Upon the addition of Nb to TiO₂ (WI), the amount of acidity decreased to 556.7 μmol/g due to the Nb coverage of the TiO₂ surface. However, a shoulder is observed at 410 °C, indicating the generation of stronger acidic sites. Furthermore, a comparison of both WI and SG samples reveals that in the WI sample, the shoulder is shifted to 385 °C and for the SG sample to 320 °C, and the overall acidity is higher (212 μmol/g) than in SG (146.2 μmol/g). In the case of the WI sample, Nb is mostly located on the surface and provides higher and stronger acidic sites than the SG sample, where a larger fraction of the Nb is expected to be located in the bulk. According to Table 3, the total amount of acidity for these catalysts follows the sequence TiO₂ > Nb5/Ti100 > Ce40/Ti100 > Nb5/Ce40/Ti100 (WI) > Nb5/Ce40/Ti100 (SG).

In situ DRIFT spectroscopy was applied to the two catalysts prepared with SG and WI methods, as well as with Ce40/Ti100 to study the interaction with the feed components NO/O₂ and NH₃. The spectra obtained after exposure to NO/O₂/He at 200 °C and flushing with He are depicted in Figure 7a. On all samples, a couple of distinct bands were observed and assigned to adsorbed NO₂ (1606–1616 cm⁻¹), bidentate nitrate (1570 and 1220 cm⁻¹), and monodentate nitrate (around 1550 and 1370 cm⁻¹) species [50,51]. All samples have in common that the bidentate nitrate species are only stable under NO/O₂ flow and vanish after He flushing. The band intensities of the remaining monodentate nitrate species on the SG and WI samples differ from those observed for the Ce40/Ti100 sample. This suggests that a part of the adsorption sites available on the latter are blocked by doping

with Nb, which is more pronounced for the WI sample. While under NO/O₂ flow, significantly more nitrate species are formed on SG compared to the WI sample, the amount of remaining adsorbates after He flushing is comparable for both catalysts. A small moiety of NO₂ is more strongly adsorbed on the SG sample and therefore also detectable after He flushing.

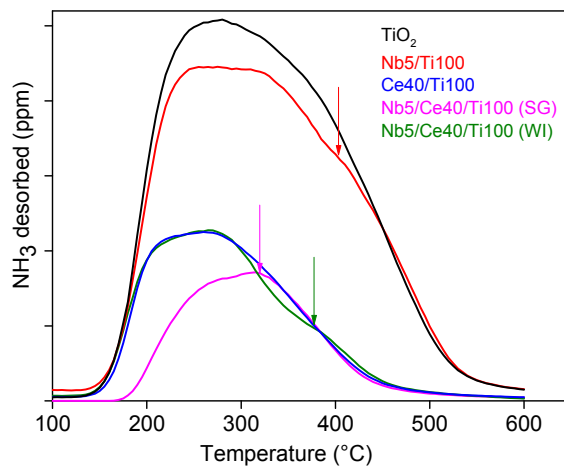


Figure 6. NH₃-TPD plots of supported Ceria-based catalysts and reference materials.

Table 3. Total amount of NH₃ desorbed in from the fresh samples.

Catalysts	Amount of NH ₃ Desorbed (μmol/g)
TiO ₂	605.7
Nb5/Ti100	556.7
Ce40/Ti100	213.4
Nb5/Ce40/Ti100 (SG)	146.2
Nb5/Ce40/Ti100 (WI)	212.7

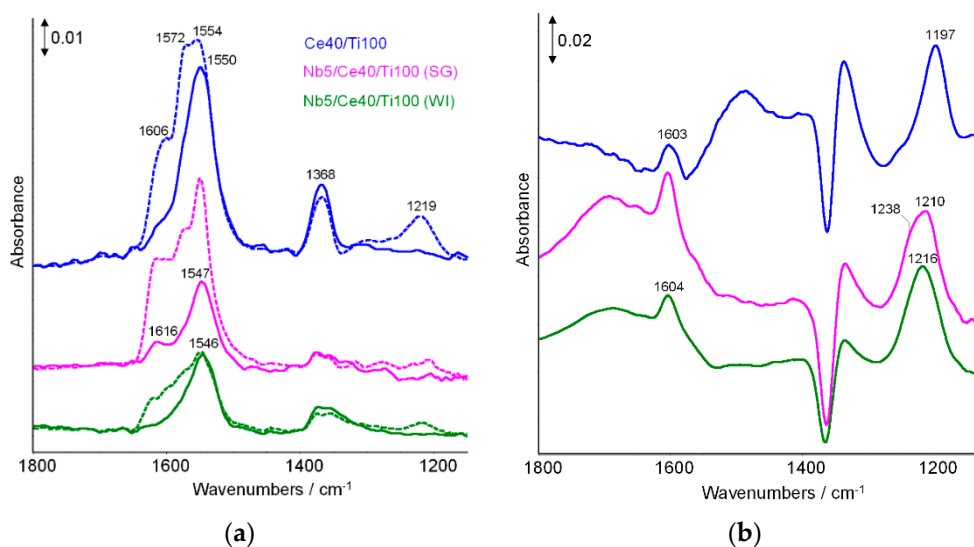


Figure 7. In situ DRIFT spectra of Ce40/Ti100, Nb5/Ce40/Ti100 (SG), and Nb5/Ce40/Ti100 (WI) measured at 200 °C after (a) NO/O₂/He adsorption (dashed lines) and subsequent flushing with He (solid lines) and (b) exposure to NH₃/He and subsequent flushing with He.

In another experiment, the catalysts were exposed to NH_3/He at $200\text{ }^\circ\text{C}$ followed by flushing with He (Figure 7b). The bands at 1604 cm^{-1} and around 1200 cm^{-1} were assigned to asymmetric and symmetric bending vibrations of NH_3 , respectively, coordinatively bound to Lewis acid sites [52]. Compared to the Ce40/Ti100 sample, the symmetric bending vibration (1197 cm^{-1}) is shifted to higher wavenumbers for the SG and WI samples (around 1216 cm^{-1}), while the band intensities slightly increase. This points to a change of the strength and amount of acidic sites caused by Nb doping. The intensities of the bands around 1216 cm^{-1} are similar for the SG and WI catalysts, indicating a comparable amount of Lewis sites. However, for the SG catalyst, the band positions slightly differ. Here, a shoulder at 1238 cm^{-1} is observed besides the main band at 1209 cm^{-1} , which suggests the appearance of Lewis sites with different strengths. Both experiments show that the introduction of Nb enhances the amount and strength of acid sites and therefore the ability for NH_3 activation, as well as for NO oxidation, which are beneficial for good NH_3 -SCR activity in the temperature range below $250\text{ }^\circ\text{C}$.

2.2.3. Redox Properties (XPS and H_2 -TPR)

It is well known that the surface composition and oxidation states of catalysts are very important for the NH_3 -SCR reaction, as they can remarkably influence the adsorption and activation of reactant molecules. Therefore, the surface properties of these catalysts were investigated by XPS and the deconvoluted spectra are shown in Figure 8 and the atomic ratio percentage of Ce, Nb, and oxygen species are listed in Table 4.

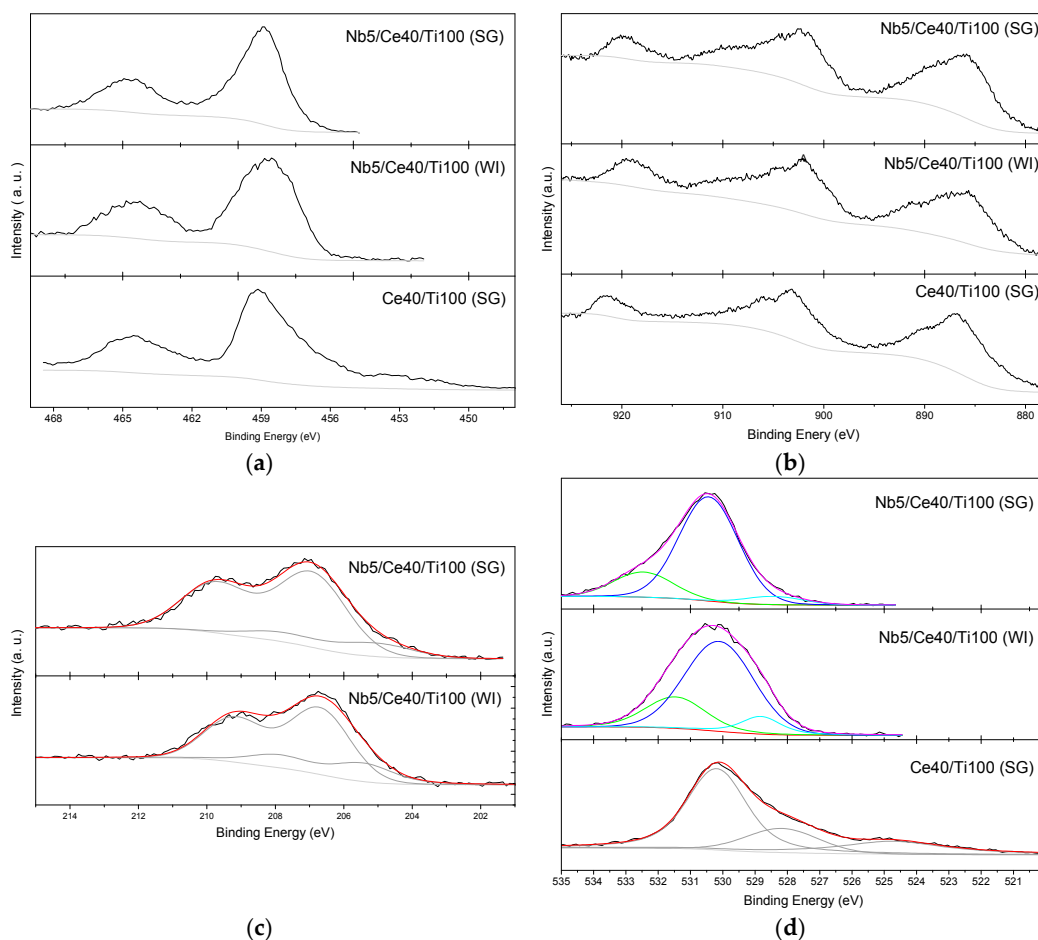


Figure 8. XPS data of the Ceria-containing catalysts: (a) Ti 2p, (b) Ce 3d, (c) Nb 3d, and (d) O 1s.

Table 4. Surface composition and element ratios of the supported Ceria-containing catalysts calculated from XPS.

Catalysts	Concentration (atom%)				Atomic Ratio (%)		
	Ce	Nb	Ti	O	Nb/(Ce + Ti)	Ce/(Ce + Ti)	O _α /(O _α + O _β)
Nb5/Ce40/Ti100 (WI)	5.2	3.5	16.7	74.7	15.9	23.6	24.6
Nb5/Ce40/Ti100 (SG)	7.7	3.2	17.1	72.0	12.7	31.2	19.6
Ce40/Ti100 (SG)	9.8	-	21.1	69.1	-	31.6	-

The Ti 2p region is dominated by two main peaks around 459 and 464 eV due to 2p_{3/2} and 2p_{1/2} contribution (Figure 8a). The spectra exhibit different symmetries and full widths at half maximum, reflecting the different local environments of Ti atoms according to the preparation method used.

The Ce 3d XPS spectra (Figure 8b) exhibit a very broad signal in the region with binding energies between 880 and 917 eV. The XPS spectra for fully oxidized Ce⁴⁺ and fully reduced Ce³⁺ reveal six respective four peaks at similar energy values. In the literature, the quantitative estimation of relative amounts of Ce⁴⁺ and Ce³⁺ is reported by fitting a linear combination of reference materials. But in the present study, the peaks are too broad for reliable deconvolution [53].

Nb 3d XPS spectra are dominated by two contributions around 206.9 and 209.7 eV that can be ascribed to Nb 3d_{5/2} and Nb 3d_{3/2}, respectively (Figure 8c). With respect to the 3d_{5/2} peak, a second contribution at a lower binding energy was detected. The energy shift is 1.9 eV for the SG sample and 1.3 eV for the WI sample, testifying to the role of different preparation methods on Nb electronic structure.

The O 1s spectra show a main signal for Ce40/Ti100 in all the samples with a maximum in the range of 530.1–530.4 eV (Figure 8d), which could be caused by lattice oxygen species named as O_β. The other signal at 528.1–528.9 eV was assigned to the oxygen ions in CeO₂ [37,54]. The signals at 531.5 and 532.1 eV for Nb5/Ce40Ti100 (WI) and (SG), respectively, are denoted as O_α, representing chemisorbed oxygen fixed on defective sites such as oxygen vacancies. The relative ratio of O_α/(O_α + O_β) is quantified based on the areas of O_α and O_β (Table 4). Accordingly, the amount of chemisorbed oxygen was higher in the WI sample (24.6%) than in the SG sample (19.6%). This could be due to the formation of Ce³⁺ as a result of the Ce-O-Nb unit, which forms charge imbalance and oxygen vacancies. These sites can promote the oxidation of NO to NO₂, resulting in high SCR activity. That is the reason why the WI sample showed more activity compared to the SG sample. It must be noted that this activation effect of Nb is only relevant for the oxygen atoms in Ceria next to Nb [29,37]. This can also explain why upon the addition of Nb via WI preparation, the amount of reducible surface species is increased, as will be discussed later by means of TPR results.

Since the redox properties are crucial for the activity of the NH₃-SCR catalyst, H₂-TPR was carried out to compare the reducibility of the prepared catalysts (Figure 9). The H₂-TPR profiles of all Ce, Ti, and Nb containing catalysts exhibit three reduction peaks between 400 and 900 °C. The low-temperature peak around 500 °C and the high-temperature peak around 800 °C can be attributed to the reduction of surface dispersed CeO₂ and bulk-like CeO₂, respectively [55,56]. Previous research [37,42] indicated that NbO_x reduction partly overlaps with CeO₂ reduction and therefore it is hard to distinguish the reduction peaks of NbO_x at high temperatures. The mid-reduction peak at 584 °C may be assigned to the reduction of Ce-O-Ti species, which form via the interaction of CeO₂ and TiO₂. Comparing Ce40Ti100 (SG) with both Nb containing catalysts suggests that Nb addition increases the reduction temperature. On the other hand, the catalyst Nb/Ce40/Ti100 (WI) shows enhanced reduction of the surface Ce⁴⁺ species as the related peak intensity in the impregnated sample is highest. This indicates that a synergetic effect between Ce and Nb increases the amount of oxygen vacancies due to the charge imbalance between Nb⁵⁺ and Ce⁴⁺ on Nb–O–Ce interfaces, as reported in literature [30,42], generating more active oxygen for the SCR reaction, as has been discussed by means of XPS data above.

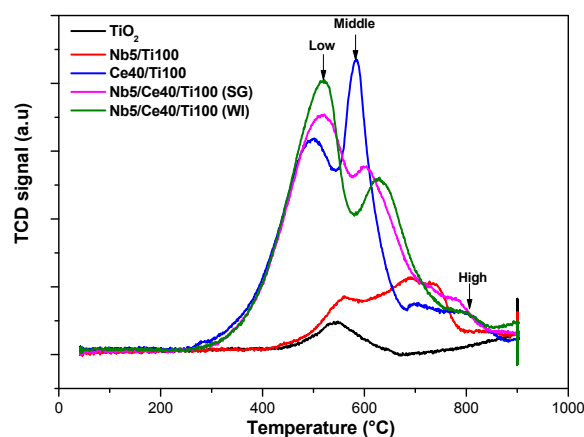


Figure 9. H₂-TPR profiles of the fresh samples.

The H₂ consumption of these supported Ceria-based catalysts is summarized in Table 5. The actual H₂ consumption of the Ce40/Ti100, Nb5/Ce40/Ti100 (SG), and (WI) catalysts is slightly higher than the theoretical H₂ consumption. It is possible that part of TiO₂ is also reduced to form Ti³⁺. All the above features are considered beneficial for the excellent SCR activity.

Table 5. H₂ consumption calculated from temperature-programmed reduction (TPR).

Catalysts	H ₂ Consumption (mmol·g ⁻¹)	
	Experimental	Theoretical
Ce40/Ti100	1548	1401
Nb5/Ce40/Ti100 (SG)	1509	1343
Nb5/Ce40/Ti100 (WI)	1455	1319

3. Materials and Methods

3.1. Catalyst Preparation

All the chemicals used in this study were supplied by Sigma-Aldrich Chemie GmbH, Munich, Germany with purities of 98–99%. Pure TiO₂ support was synthesized by a sol-gel method using Ti(IV) isopropoxide and anhydrous ethanol as the precursor. Next, ethyl acetoacetate (EAcAc) used as a complexing agent was added to the solution under stirring at room temperature. Finally, a solution of HNO₃ (0.1 M) was added drop-wise and stirred until a yellow gel was formed. The gel was extracted with supercritical ethanol in an autoclave ($T = 245\text{ }^{\circ}\text{C}$, $p = 60\text{ bar}$). The resulting product was calcined under O₂ flow at 500 °C for 3 h (heating rate 3 K/min).

The Ce40/Ti100 sample (molar ratio 0.4:1) was prepared by adding (NH₄)₂Ce(NO₃)₆ dissolved in anhydrous ethanol to the above Ti precursor solution at 60 °C until complete dissolution. For preparation of Nb5/Ce40/Ti100 (SG), NbCl₅ dissolved in anhydrous ethanol was added. Further processing was conducted as described for TiO₂.

The Nb5/Ti100 (WI) and Nb5/Ce40/Ti100 (WI) catalysts were synthesized by impregnating the as-received pure TiO₂ and Ce40/Ti100 powders, respectively, with NbCl₅ and anhydrous ethanol. The nominal loadings of Nb were 5 wt %.

3.2. Activity Measurement

The NH₃-SCR activity measurement was carried out in a fixed-bed quartz reactor (i. d. = 10 mm, length = 150 mm) from 150 to 400 °C at atmospheric pressure with 100 mg of catalyst (sieved in the range 315–710 μm). The feed gas consisted of 1000 ppm of NO, 1000 ppm of NH₃, 5 vol % of O₂

(8 vol % of water if used), and helium as the balance at a 100 mL/min total flow rate. The modified space velocity (GHSV) for activity measurement was kept at 60,000 mL·g⁻¹·h⁻¹. Before each test, the catalyst was pretreated with 5% O₂ in helium at 500 °C for 30 min. The analysis of N₂, N₂O, and O₂ in the product mixture was performed using on-line gas chromatography (HP 6890) employing a molecular sieve 5A column. Simultaneously, NO, NO₂, and NH₃ concentrations in the product stream were continuously monitored by a multigas sensor (Limas 11HW, ABB, Mannheim, Germany). The concentrations of NO, N₂O, and NO₂ were measured in ppm. The continuous reactor was kept for 1 h in steady state at each chosen reaction temperature. The NH₃-SCR activity (NO_x conversion) of catalysts was calculated using Equation (1) and the N₂ selectivity was calculated using Equation (2):

$$NOx_{Conv.}\% = \frac{(NO + NO_2)_{in} - (NO + NO_2)_{out}}{(NO + NO_2)_{in}} \times 100 \quad (1)$$

$$S_{N_2}\% = 1 - \frac{2 * N_2O}{(((NO + NO_2)_{in} - (NO + NO_2)_{out}) + (NH_{3in} - NH_{3out}))} \times 100 \quad (2)$$

As all nitrogen-containing gaseous reactants were quantified, it was possible to calculate the nitrogen balance. Typically, the values ranged from 94 to 100%. To investigate the long-term stability and the effect of water (8 vol %) on the catalyst performance, the temperature was set to 200 °C.

3.3. Catalyst Characterization

The elemental compositions were determined by inductively coupled plasma optical emission spectroscopy (ICP-OES) using a 715-ES ICP emissions spectrometer (Varian, Palo Alto, CA, USA). The samples were digested in a mixture of HF and aqua regia and then treated in a microwave assisted sample preparation apparatus at 200 °C and 60 bar.

BET surface area and pore volume of the prepared catalysts were measured from nitrogen adsorption isotherms measured at -196 °C (Micromeritics ASAP 2010). Before the measurement, each sample was degassed at 200 °C for 4 h. The average pore diameters were calculated from the desorption branch of the isotherm using the BJH method.

XRD powder patterns were recorded on a X'Pert diffractometer (Panalytical, Almelo, The Netherlands) equipped with a Xcelerator detector, used with automatic divergence slits and Cu Kα1/α2 radiation (40 kV, 40 mA; λ = 0.015406 nm, 0.0154443 nm). Cu beta-radiation was excluded by using nickel filter foil. The measurements were performed in 0.0167° steps and 25 s of data collecting time per step. The samples were mounted on silicon zero background holders. The collected data were converted from automatic divergence slits to fixed divergence slits (0.25°) before data analysis to obtain the correct intensities. Peak positions and profile were fitted with the Pseudo-Voigt function using the HighScore Plus software package (Panalytical, Almelo, The Netherlands). Phase identification was done by using the PDF-2 database of the International Center of Diffraction Data (ICDD). Crystallite size was calculated by applying the Scherrer equation using the integral breadth under the assumption of spherically shaped crystallites. K was set to 1.0747.

The Raman spectra of the samples were collected on a Via Raman microscope (Renishaw, Wotton-under-edge, UK) using a 633 nm laser with a laser power between 0.81 and 1.61 mW. The samples were mounted onto object slides and an objective with a magnification of 50 was applied. To prove the homogeneity of the materials, spectra were acquired at different points of the sample.

X-ray photoelectron spectra were performed with a Thermo ESCALAB 220 iXL spectrometer (ThermoFisher, Walham, MA, USA) at room temperature using monochromatic AlKα radiation. Binding energies were corrected to C-C contribution at 284.8 eV in the C1s region. Signal intensities were normalized using the sensitivity factors of Scofield [57] and the transmission function of the spectrometer.

In situ DRIFT spectra were measured on a Nicolet 6700 FTIR spectrometer using a high-temperature reaction cell (Harrick) equipped with a temperature programmer (Eurotherm) and

connected to a gas-dosing device with mass flow controllers (Bronkhorst). The catalyst samples were pretreated for 1 h at 300 °C in air, cooled to a reaction temperature of 200 °C in He, and subsequently exposed to a flow (30 mL/min) of 1000 ppm NO, 4% O₂, balanced with He or 1000 ppm NH₃, balanced with He, respectively, for 45 min. Then, the cell was flushed with He for 20 min. Generally, subtracted spectra were evaluated, obtained by subtraction of the spectrum recorded after pretreatment and He flushing at reaction temperature from the respected adsorbate spectra.

TPR measurement was done using a Autochem II 2920 instrument (Micromeritics, Aachen, Germany). A 70 mg sample was loaded into a U-shaped quartz reactor and heated from RT to 400 °C with 10 K/min in 5% O₂/He (50 mL/min) for 30 min at 400 °C to remove any adsorbed species. Then, the system cooled down to RT in a flow of 5% O₂/He. The TPR run was carried out from RT to 900 °C in a 5% H₂/Ar flow (50 mL/min) with a heating rate of 10 K/min. The hydrogen consumption was continuously recorded using a thermal conductivity detector and quantitatively analyzed.

Temperature-programmed desorption of ammonia (TPD-NH₃) was performed by inserting a 230 mg sample into a home-made quartz-tube reactor. The samples were flushed in He (100 mL/min) for 1 h at 100 °C. Then, the sample was exposed to 1000 ppm NH₃/He (100 mL/min) for 1 h at 100 °C. Afterwards, physisorbed ammonia was removed by flushing the sample with He (100 mL/min) for 1 h at 100 °C. The sample was then ramped to 600 °C at a heating rate of 10 K/min in He (100 mL/min). The temperature was held at 600 °C for 30 min. The amount of ammonia desorbed with temperature was continuously monitored by a multigas sensor (Limas 11HW, ABB, Mannheim, Germany). The amount of acidity was calculated based on peak area integration.

4. Conclusions

The combination of three metal oxides (CeO₂, TiO₂, and Nb₂O₅) was chosen as the catalyst system for the SCR reaction and the effects of structure (core-shell vs bulk catalyst) and Nb doping on the catalytic activity were studied. Nb doped Ce40/Ti100 catalysts prepared by two methods WI and SG were used in the NH₃-SCR reaction. Nb5/Ce40/Ti100 (WI) showed the highest SCR activity (95%) at 200 °C in the absence of H₂O at GHSV = 60,000 h⁻¹. To our knowledge, this is among the best results for catalysts based on this ternary system for an intermediate temperature SCR. The stability of the catalysts was tested in the presence of H₂O, and the catalysts showed a loss of 22–27% in conversion. Nb5/Ce40/Ti100 (WI) exhibited higher conversions compared to the SG sample and showed a less pronounced deactivation over 12 h. It is noteworthy that at temperatures below 250 °C, byproduct formation is completely suppressed, which is advantageous compared to Mn-based systems. The latter tend to over-oxidize NO. On the other side, the Nb/Ce/Ti system could be an alternative to the V₂O₅/TiO₂ system, due to higher activity, particularly if it would be able to avoid the oxidation of SO₂ to SO₃ (as known for V₂O₅/TiO₂). The catalyst might be preferably applicable for intermediate temperature SCR. The results of BET, XRD, Raman, XPS, H₂-TPR, in situ DRIFT, and TPD-NH₃ studies clearly evidenced that the addition of Nb via wet impregnation leads to a high Nb concentration on the surface, which has a prominent effect on acidity, as well as the amount of adsorbed oxygen, with the latter resulting in a good redox ability. Second, the addition of Niobium improved the dispersion of Cerium, and third the coexistence of Nb and Ce/Ti species was of essential importance for a high NH₃-SCR performance. These are the key factors for the good performance of the Nb-modified Ce-based catalyst in SCR. This means that both the preparation method (core-shell versus bulk catalyst) and metal addition are essential for generating a good catalyst which is active and selective.

Author Contributions: J.M., H.A., M.M., and U.A. conceived and designed the experiments; J.M. and R.E. performed the catalyst tests and analyzed the data; H.A. performed the TPR and NH₃-TPD analyses and analyzed the data; R.E. performed the BET measurements; H.L. performed the XRD measurements; G.A. performed the XPS measurements; N.R., U.B., and S.K. performed the RAMAN and DRIFTS experiments and analyzed the data; J.M., H.A., and U.A. wrote the paper.

Acknowledgments: The authors are grateful to Karin Struve for ICP measurements and acknowledge the staff of LIKAT and LCMC for all the help in discussing the results. J.M. acknowledges the staff of LIKAT and LCMC for

all the efforts and help they have given. The publication of this article was funded by the Open Access Fund of the Leibniz Association.

Conflicts of Interest: The authors declare no conflict of interest.

References

1. Skalska, K.; S Miller, J.; Ledakowicz, S. Trends in NO_x abatement: A review. *Sci. Total Environ.* **2010**, *408*, 3976–3989. [[CrossRef](#)] [[PubMed](#)]
2. Busca, G.; Lietti, L.; Ramis, G.; Berti, F. Chemical and mechanistic aspects of the selective catalytic reduction of NO_x by ammonia over oxide catalysts: A review. *Appl. Catal. B Environ.* **1998**, *18*, 1–36. [[CrossRef](#)]
3. Lietti, L.; Nova, I.; Forzatti, P. Selective catalytic reduction (SCR) of NO by NH₃ over TiO₂-supported V₂O₅-WO₃ and V₂O₅-MoO₃ catalysts. *Top. Catal.* **2000**, *11*, 111–122. [[CrossRef](#)]
4. Long, R.Q.; Yang, R.T. Fe-ZSM-5 for Selective Catalytic Reduction of NO with NH₃: A Comparative Study of Different Preparation Techniques. *Catal. Lett.* **2001**, *74*, 201–205. [[CrossRef](#)]
5. Delahay, G.; Valade, D.; Guzmán-Vargas, A.; Coq, B. Selective catalytic reduction of nitric oxide with ammonia on Fe-ZSM-5 catalysts prepared by different methods. *Appl. Catal. B Environ.* **2005**, *55*, 149–155. [[CrossRef](#)]
6. Ayari, F.; Mhamdi, M.; Álvarez-Rodríguez, J.; Ruiz, A.R.G.; Delahay, G.; Ghorbel, A. Selective catalytic reduction of NO with NH₃ over Cr-ZSM-5 catalysts: General characterization and catalysts screening. *Appl. Catal. B Environ.* **2013**, *134–135*, 367–380. [[CrossRef](#)]
7. Forzatti, P. Present status and perspectives in de-NO_x SCR catalysis. *Appl. Catal. A Gen.* **2001**, *222*, 221–236. [[CrossRef](#)]
8. Michalow-Mauke, K.A.; Lu, Y.; Kowalski, K.; Graule, T.; Nachttegaal, M.; Kröcher, O.; Ferri, D. Flame-Made WO₃/CeO_x-TiO₂ Catalysts for Selective Catalytic Reduction of NO_x by NH₃. *ACS Catal.* **2015**, *5*, 5657–5672. [[CrossRef](#)]
9. Ding, S.; Liu, F.; Shi, X.; Liu, K.; Lian, Z.; Xie, L.; He, H. Significant Promotion Effect of Mo Additive on a Novel Ce-Zr Mixed Oxide Catalyst for the Selective Catalytic Reduction of NO_x with NH₃. *ACS Appl. Mater. Interfaces* **2015**, *7*, 9497–9506. [[CrossRef](#)] [[PubMed](#)]
10. Liu, J.; Li, X.; Zhao, Q.; Ke, J.; Xiao, H.; Lv, X.; Liu, S.; Tadé, M.; Wang, S. Mechanistic investigation of the enhanced NH₃-SCR on cobalt-decorated Ce-Ti mixed oxide: In situ FTIR analysis for structure-activity correlation. *Appl. Catal. B Environ.* **2017**, *200*, 297–308. [[CrossRef](#)]
11. Liu, C.; Chen, L.; Li, J.; Ma, L.; Arandiyán, H.; Du, Y.; Xu, J.; Hao, J. Enhancement of Activity and Sulfur Resistance of CeO₂ Supported on TiO₂-SiO₂ for the Selective Catalytic Reduction of NO by NH₃. *Environ. Sci. Technol.* **2012**, *46*, 6182–6189. [[CrossRef](#)] [[PubMed](#)]
12. Krishna, K.; B F Seijger, G.; M van den Bleek, C.; Calis, H.P.A. Very active CeO₂-zeolite catalysts for NO_x reduction with NH₃. *Chem. Commun.* **2002**, *18*, 2030–2031. [[CrossRef](#)]
13. Jin, R.; Liu, Y.; Wu, Z.; Wang, H.; Gu, T. Relationship between SO₂ poisoning effects and reaction temperature for selective catalytic reduction of NO over Mn-Ce/TiO₂ catalyst. *Catal. Today* **2010**, *153*, 84–89. [[CrossRef](#)]
14. Xu, W.; He, H.; Yu, Y. Deactivation of a Ce/TiO₂ Catalyst by SO₂ in the Selective Catalytic Reduction of NO by NH₃. *J. Phys. Chem. C* **2009**, *113*, 4426–4432. [[CrossRef](#)]
15. Xu, W.; Yu, Y.; Zhang, C.; He, H. Selective catalytic reduction of NO by NH₃ over a Ce/TiO₂ catalyst. *Catal. Commun.* **2008**, *9*, 1453–1457. [[CrossRef](#)]
16. Chen, L.; Li, J.; Ge, M.; Zhu, R. Enhanced activity of tungsten modified CeO₂/TiO₂ for selective catalytic reduction of NO_x with ammonia. *Catal. Today* **2010**, *153*, 77–83. [[CrossRef](#)]
17. Peng, Y.; Li, K.; Li, J. Identification of the active sites on CeO₂-WO₃ catalysts for SCR of NO_x with NH₃: An in situ IR and Raman spectroscopy study. *Appl. Catal. B Environ.* **2013**, *140–141*, 483–492. [[CrossRef](#)]
18. Ma, Z.; Weng, D.; Wu, X.; Si, Z. Effects of WO_x modification on the activity, adsorption and redox properties of CeO₂ catalyst for NO_x reduction with ammonia. *J. Environ. Sci.* **2012**, *24*, 1305–1316. [[CrossRef](#)]
19. Shan, W.; Liu, F.; He, H.; Shi, X.; Zhang, C. A superior Ce-W-Ti mixed oxide catalyst for the selective catalytic reduction of NO_x with NH₃. *Appl. Catal. B Environ.* **2012**, *115–116*, 100–106. [[CrossRef](#)]
20. Shan, W.; Liu, F.; He, H.; Shi, X.; Zhang, C. Novel Cerium-tungsten mixed oxide catalyst for the selective catalytic reduction of NO_x with NH₃. *Chem. Commun.* **2011**, *47*, 8046–8048. [[CrossRef](#)] [[PubMed](#)]
21. Chen, L.; Li, J.; Ge, M. DRIFT Study on Cerium-Tungsten/Titanium Catalyst for Selective Catalytic Reduction of NO_x with NH₃. *Environ. Sci. Technol.* **2010**, *44*, 9590–9596. [[CrossRef](#)] [[PubMed](#)]

22. Peng, Y.; Liu, Z.; Niu, X.; Zhou, L.; Fu, C.; Zhang, H.; Li, J.; Han, W. Manganese doped CeO₂-WO₃ catalysts for the selective catalytic reduction of NO_x with NH₃: An experimental and theoretical study. *Catal. Commun.* **2012**, *19*, 127–131. [[CrossRef](#)]
23. Gu, T.; Liu, Y.; Weng, X.; Wang, H.; Wu, Z. The enhanced performance of Ceria with surface sulfation for selective catalytic reduction of NO by NH₃. *Catal. Commun.* **2010**, *12*, 310–313. [[CrossRef](#)]
24. Si, Z.; Weng, D.; Wu, X.; Yang, J.; Wang, B. Modifications of CeO₂-ZrO₂ solid solutions by nickel and sulfate as catalysts for NO reduction with ammonia in excess O₂. *Catal. Commun.* **2010**, *11*, 1045–1048. [[CrossRef](#)]
25. Si, Z.; Weng, D.; Wu, X.; Ma, Z.; Ma, J.; Ran, R. Lattice oxygen mobility and acidity improvements of NiO-CeO₂-ZrO₂ catalyst by sulfation for NO_x reduction by ammonia. *Catal. Today* **2013**, *201*, 122–130. [[CrossRef](#)]
26. Casapu, M.; Kröcher, O.; Elsener, M. Screening of doped MnO_x-CeO₂ catalysts for low-temperature NO-SCR. *Appl. Catal. B Environ.* **2009**, *88*, 413–419. [[CrossRef](#)]
27. Casapu, M.; Kröcher, O.; Mehring, M.; Nachtgeal, M.; Borca, C.; Harfouche, M.; Grolimund, D. Characterization of Nb-Containing MnO_x-CeO₂ Catalyst for Low-Temperature Selective Catalytic Reduction of NO with NH₃. *J. Phys. Chem. C* **2010**, *114*, 9791–9801. [[CrossRef](#)]
28. Casapu, M.; Bernhard, A.; Peitz, D.; Mehring, M.; Elsener, M.; Kröcher, O. A Niobia-Ceria based multi-purpose catalyst for selective catalytic reduction of NO_x, urea hydrolysis and soot oxidation in diesel exhaust. *Appl. Catal. B Environ.* **2011**, *103*, 79–84. [[CrossRef](#)]
29. Qu, R.; Gao, X.; Cen, K.; Li, J. Relationship between structure and performance of a novel Cerium-Niobium binary oxide catalyst for selective catalytic reduction of NO with NH₃. *Appl. Catal. B Environ.* **2013**, *142–143*, 290–297. [[CrossRef](#)]
30. Ma, Z.; Weng, D.; Wu, X.; Si, Z.; Wang, B. A novel Nb-Ce/WO_x-TiO₂ catalyst with high NH₃-SCR activity and stability. *Catal. Commun.* **2012**, *27*, 97–100. [[CrossRef](#)]
31. Si, Z.; Weng, D.; Wu, X.; Ran, R.; Ma, Z. NH₃-SCR activity, hydrothermal stability, sulfur resistance and regeneration of Ce_{0.75}Zr_{0.25}O₂-PO₄3-catalyst. *Catal. Commun.* **2012**, *17*, 146–149. [[CrossRef](#)]
32. Yu, J.; Si, Z.; Chen, L.; Wu, X.; Weng, D. Selective catalytic reduction of NO_x by ammonia over phosphate-containing Ce_{0.75}Zr_{0.25}O₂ solids. *Appl. Catal. B Environ.* **2015**, *163*, 223–232. [[CrossRef](#)]
33. Liu, Z.; Zhang, S.; Li, J.; Ma, L. Promoting effect of MoO₃ on the NO_x reduction by NH₃ over CeO₂/TiO₂ catalyst studied with in situ DRIFTS. *Appl. Catal. B Environ.* **2014**, *144*, 90–95. [[CrossRef](#)]
34. Gao, X.; Jiang, Y.; Fu, Y.; Zhong, Y.; Luo, Z.; Cen, K. Preparation and characterization of CeO₂/TiO₂ catalysts for selective catalytic reduction of NO with NH₃. *Catal. Commun.* **2010**, *11*, 465–469. [[CrossRef](#)]
35. Brayner, R.; Ciuparu, D.; da Cruz, G.M.; Fiévet-Vincent, F.; Bozon-Verduraz, F. Preparation and characterization of high surface area Niobia, Ceria-Niobia and Ceria-Zirconia. *Catal. Today* **2000**, *57*, 261–266. [[CrossRef](#)]
36. Yashiro, K.; Suzuki, T.; Kaimai, A.; Matsumoto, H.; Nigara, Y.; Kawada, T.; Mizusaki, J.; Sfeir, J.; Van herle, J. Electrical properties and defect structure of Niobia-doped Ceria. *Solid State Ion.* **2004**, *175*, 341–344. [[CrossRef](#)]
37. Zhao, B.; Ran, R.; Guo, X.; Cao, L.; Xu, T.; Chen, Z.; Wu, X.; Si, Z.; Weng, D. Nb-modified Mn/Ce/Ti catalyst for the selective catalytic reduction of NO with NH₃ at low temperature. *Appl. Catal. A Gen.* **2017**, *545*, 64–71. [[CrossRef](#)]
38. Qi, G.; Yang, R.T. A superior catalyst for low-temperature NO reduction with NH₃. *Chem. Commun.* **2003**, *7*, 848–849. [[CrossRef](#)]
39. Shen, Q.; Zhang, L.; Sun, N.; Wang, H.; Zhong, L.; He, C.; Wei, W.; Sun, Y. Hollow MnO_x-CeO₂ mixed oxides as highly efficient catalysts in NO oxidation. *Chem. Eng. J.* **2017**, *322*, 46–55. [[CrossRef](#)]
40. Lian, Z.; Liu, F.; He, H.; Liu, K. Nb-doped VO_x/CeO₂ catalyst for NH₃-SCR of NO_x at low temperatures. *RSC Adv.* **2015**, *5*, 37675–37681. [[CrossRef](#)]
41. Li, Y.; Li, Y.; Wan, Y.; Zhan, S.; Guan, Q.; Tian, Y. Structure-performance relationships of MnO₂ nanocatalyst for the low-temperature SCR removal of NO_x under ammonia. *RSC Adv.* **2016**, *6*, 54926–54937. [[CrossRef](#)]
42. Ma, Z.; Wu, X.; Si, Z.; Weng, D.; Ma, J.; Xu, T. Impacts of Niobia loading on active sites and surface acidity in NbO_x/CeO₂-ZrO₂ NH₃-SCR catalysts. *Appl. Catal. B Environ.* **2015**, *179*, 380–394. [[CrossRef](#)]
43. Langford, J.I.; Wilson, A.J.C. Scherrer after sixty years: A survey and some new results in the determination of crystallite size. *J. Appl. Crystallogr.* **1978**, *11*, 102–113. [[CrossRef](#)]
44. Yao, X.; Zhang, L.; Li, L.; Liu, L.; Cao, Y.; Dong, X.; Gao, F.; Deng, Y.; Tang, C.; Chen, Z.; et al. Investigation of the structure, acidity, and catalytic performance of CuO/Ti_{0.95}Ce_{0.05}O₂ catalyst for the selective catalytic reduction of NO by NH₃ at low temperature. *Appl. Catal. B Environ.* **2014**, *150–151*, 315–329. [[CrossRef](#)]

45. Liu, L.; Zhao, H.; Andino, J.M.; Li, Y. Photocatalytic CO₂ Reduction with H₂O on TiO₂ Nanocrystals: Comparison of Anatase, Rutile, and Brookite Polymorphs and Exploration of Surface Chemistry. *ACS Catal.* **2012**, *2*, 1817–1828. [[CrossRef](#)]
46. Balachandran, U.; Eror, N.G. Raman spectra of Titanium dioxide. *J. Solid State Chem.* **1982**, *42*, 276–282. [[CrossRef](#)]
47. Kong, L.; Gregg, D.J.; Karatchevtseva, I.; Zhang, Z.; Blackford, M.G.; Middleburgh, S.C.; Lumpkin, G.R.; Triani, G. Novel Chemical Synthesis and Characterization of CeTi₂O₆ Brannerite. *Inorg. Chem.* **2014**, *53*, 6761–6768. [[CrossRef](#)] [[PubMed](#)]
48. Fu, M.; Wei, L.; Li, Y.; Zhou, X.; Hao, S.; Li, Y. Surface charge tuning of Ceria particles by Titanium doping: Towards significantly improved polishing performance. *Solid State Sci.* **2009**, *11*, 2133–2137. [[CrossRef](#)]
49. Fang, C.; Zhang, D.; Cai, S.; Zhang, L.; Huang, L.; Li, H.; Maitarad, P.; Shi, L.; Gao, R.; Zhang, J. Low-temperature selective catalytic reduction of NO with NH₃ over nanoflaky MnO_x on carbon nanotubes in situ prepared via a chemical bath deposition route. *Nanoscale* **2013**, *5*, 9199–9207. [[CrossRef](#)] [[PubMed](#)]
50. Dines, T.J.; Rochester, C.H.; Ward, A.M. Infrared and Raman study of the adsorption of NH₃, pyridine, NO and NO₂ on anatase. *J. Chem. Soc. Faraday Trans.* **1991**, *87*, 643–651. [[CrossRef](#)]
51. Hadjiivanov, K.I. Identification of Neutral and Charged N_xO_y Surface Species by IR Spectroscopy. *Catal. Rev.* **2000**, *42*, 71–144. [[CrossRef](#)]
52. Davydov, A. The Nature of Oxide Surface Centers. In *Molecular Spectroscopy of Oxide Catalyst Surfaces*; John Wiley & Sons: Hoboken, NJ, USA, 2003.
53. Mullins, D.R. The surface chemistry of Cerium oxide. *Surf. Sci. Rep.* **2015**, *70*, 42–85. [[CrossRef](#)]
54. Reddy, B.M.; Khan, A. Nanosized CeO₂-SiO₂, CeO₂-TiO₂, and CeO₂-ZrO₂ Mixed Oxides: Influence of Supporting Oxide on Thermal Stability and Oxygen Storage Properties of Ceria. *Catal. Surv. Asia* **2005**, *9*, 155–171. [[CrossRef](#)]
55. Li, P.; Xin, Y.; Li, Q.; Wang, Z.; Zhang, Z.; Zheng, L. Ce-Ti Amorphous Oxides for Selective Catalytic Reduction of NO with NH₃: Confirmation of Ce-O-Ti Active Sites. *Environ. Sci. Technol.* **2012**, *46*, 9600–9605. [[CrossRef](#)] [[PubMed](#)]
56. Neri, G.; Pistone, A.; Milone, C.; Galvagno, S. Wet air oxidation of p-coumaric acid over promoted Ceria catalysts. *Appl. Catal. B Environ.* **2002**, *38*, 321–329. [[CrossRef](#)]
57. Scofield, J.H. Hartree-Slater subshell photoionization cross-sections at 1254 and 1487 eV. *J. Electron Spectrosc. Relat. Phenom.* **1976**, *8*, 129–137. [[CrossRef](#)]



© 2018 by the authors. Licensee MDPI, Basel, Switzerland. This article is an open access article distributed under the terms and conditions of the Creative Commons Attribution (CC BY) license (<http://creativecommons.org/licenses/by/4.0/>).